Thermal expansion of plagioclase feldspars

Thermal expansion of plagioclase feldspars

M. Tribaudino[1], R.J. Angel[2], F. Cámara [3], F. Nestola[4], D. Pasqual[4], I. Margiolaki[5]

[1]Dipartimento di Scienze della Terra, Università di Parma, Viale G.P. Usberti 157/A, I-43100 Parma, Italy
[2]Department of Geosciences, Virginia Polytechnic Institute and State University, Blacksburg, Virginia 24061, U.S.A.
[3]CNR-Istituto di Geoscienze e Georisorse, U.O.S. Pavia, via Ferrata 1, 27100 Pavia, Italy.
[4]Dipartimento di Geoscienze, Università di Padova, Via Giotto 1, I-35137 Padova, Italy.
5 European Synchrotron Radiation Facility (ESRF), B.P. 220, F-38043, Grenoble, France

For submission to: Contributions to Mineralogy and Petrology

Abstract: The volume thermal expansion coefficient and the anisotropy of thermal expansion were determined for nine natural feldspars with compositions, in terms of albite ($NaAlSi_3O_8$, Ab) and anorthite ($CaAl_2Si_2O_8$, An), of Ab_{100}, $An_{27}Ab_{73}$, $An_{35}Ab_{65}$, $An_{46}Ab_{54}$, $An_{60}Ab_{40}$, $An_{78}Ab_{22}$, $An_{89}Ab_{11}$, $An_{96}Ab_4$ and An_{100} by high resolution powder diffraction with a synchrotron radiation source. Unit-cell parameters were determined from 124 powder patterns of each sample, collected over the temperature range 298K – 935K. The volume thermal expansion coefficient of the samples determined by a linear fit of $V/V_0 = \alpha(T-T_0)$ varies with composition (X_{An} in mol %) as:

$$\alpha_V = 2.90(4)\cdot10^{-5} - 3.0(2)\cdot10^{-7}*X_{An} + 1.8(2)\cdot10^{-9}*X_{An}^2$$

Two empirical models for the non-linear behaviour of volume with temperature give a better fit to the experimental data. The change with composition in the a° parameter of the non-linear Holland-Powell model $V/V_0= 1+a°(T-T_0)+20a° (\sqrt{T}-\sqrt{T_0})$ is:

$$a° = 4.96(5)\cdot10^{-5} - 4.7(2)\cdot10^{-7}*X_{An} + 2.2(2)\cdot10^{-9}*X_{An}^2$$

For the Berman model, $V/V_0= a_1(T-T_0)+a_2*(T-T_0)^2$, the parameters change with composition as:

$$a_1= 2.44(15)\cdot10^{-5} - 3.1(6)\cdot10^{-7}*X_{An} + 1.8(5)\cdot10^{-9}*X_{An}^2$$

$$a_2= 9(1)\cdot10^{-9} - 4(2)\cdot10^{-11}*X_{An}$$

The thermal expansion of all plagioclases is very anisotropic, with more than 70% of the volume expansion being accommodated by a direction fairly close to the (100) plane normal, whereas perpendicular directions exhibit smaller, and in some cases slightly negative or zero, thermal expansion.

Introduction

Plagioclase feldspars are among the major constituents of the Earth's crust; they are involved in several key reactions of petrologic interest and any model used to describe phase equilibria and the structural behaviour of the crust requires the thermoelastic properties of plagioclase feldspars. The most important parameters for non-ambient behaviour are the volume dependence upon pressure (the bulk modulus) and the volume thermal expansion, and their evolution with temperature and pressure. Recent data on bulk moduli were provided by Angel (2004). By contrast, apart from very recent measurements by Hovis et al. (2010), volume thermal expansion data on plagioclase are relatively few, mostly confined to the end members, and date to the 1970s or earlier. Nonetheless, these data are currently used for thermodynamic modelling in the most widely-used data bases (e.g. Berman 1988, Holland and Powell 1998, Gottschalk 1997).

Experimental studies of the thermal expansion of plagioclase feldspars date back to Beckenkamp (1881), who determined the volume thermal expansion and the thermal strain ellipsoid of anorthite from 25 to 200°C by measuring dihedral angles between crystallographic faces. A series of dilatometric measurements on plagioclase were performed by Kozu and Ueda (1933; reported in Skinner 1966), using single crystals polished as cubes. They measured several different intermediate plagioclases, with compositions $Ab_{99}An_1$, $Ab_{77}An_{23}$, $Ab_{56}An_{44}$ and Ab_5An_{95}, up to 1000°C and found that the volume thermal expansion coefficient decreases with increasing anorthite content (Fig. 1). Dilatometric methods, reviewed in Saucier and Saplevitch (1962), were abandoned with the introduction in the early 1960s of in-situ X-ray high-temperature powder diffraction. Although most of the high temperature X-ray studies were done on the end member plagioclases (albite: Stewart and Von Limbach 1967, Grundy and Brown 1969; anorthite: Czank and Schultz 1971), the thermal expansion of plagioclases of intermediate compositions was also investigated (Stewart et al. 1966; Grundy and Brown 1974). The Grundy and Brown (1974) paper represents the only investigation by X-ray diffraction over the entire plagioclase join prior to this work and that of Hovis et al. (2010); it shows that the thermal expansion decreases from Ab to

$Ab_{50}An_{50}$, but does not change at higher anorthite contents. A comparison with earlier dilatometric data by Kozu and Ueda (1933) shows good agreement in the albite-rich part of the join, but significant differences of about 30% in the volume thermal expansion coefficients of anorthite-rich plagioclase (Figure 1). The volume thermal expansion coefficient of labradorite determined by Stewart et al. (1966) is in agreement with dilatometric data.

Diffraction methods, whether powder or single crystal, not only provide information on the volume thermal expansion but also on the anisotropy of the thermal expansion in triclinic crystals such as plagioclase feldspars. By using a strain tensor analysis it was shown (Ohashi and Finger, 1973; Willaime et al. 1974) that the thermal expansion of plagioclase feldspars was very anisotropic, but similar for all plagioclase except for end-member anorthite. One direction close to the [001] axis exhibits near-zero, or even negative thermal expansion for some compositions, and most of the volume expansion is accounted for by the expansion of a direction not far from the (100) plane normal.

After the introduction of high-temperature single-crystal diffractometry the structural changes with temperature were determined in end-member plagioclase (high and low albite: Prewitt et al 1976, Winter et al 1977, 1979; anorthite: Foit and Peacor 1974, Ghose et al 1993), and new powder diffraction studies were used to detail their phase transitions (albite: Kroll et al 1980, Brown et al 1984, Salje et al 1985, Hovis and Graeme Barber 1988; anorthite: Redfern and Salje 1987, Redfern et al 1988, Redfern 1992, Carpenter 1992). These studies were not aimed at determining the thermal expansion and involved only, or close to, the end member compositions. The literature data used in thermodynamic databases for petrologic calculations are summarised in Table 1.

In recent years, the introduction of high resolution powder diffraction at synchrotron radiation and neutron spallation sources, together with full pattern powder diffraction fitting via Rietveld analysis, enables volume data to an unprecedented precision to be obtained. This enables the detection and analysis of deviations from linear behaviour, the discrimination of subtle volume

changes driven by phase transitions and the detailed evolution of the thermal strain ellipsoid to be determined, as illustrated recently for amphiboles and pyroxenes (e.g. Tribaudino et al. 2008, Knight and Price 2008). In feldspars, to the authors knowledge, such high resolution powder diffraction has only been performed on synthetic Sr-bearing anorthite (Tribaudino et al. 2005).

In this work, we report high-resolution powder diffraction data for nine natural and well-characterized plagioclase samples measured between 298 and 935 K in order to provide updated volume thermal expansion data to be used in petrologic databases. The thermal expansion ellipsoid was also determined in order to describe the anisotropic deformation that this triclinic material undergoes with temperature.

Experimental

The high-resolution powder diffraction study was performed on nine well-characterized plagioclase samples with compositions chosen to span the plagioclase join and provide constraints on possible changes in thermal expansion associated with phase transitions. Composition, sample identification and structural state are reported in Table 2. Most of these samples were previously characterised by TEM and X-ray powder diffraction and were used for calorimetry by Carpenter et al. (1985). The crystal structures of six of the samples were determined anew for this study. Each structure was refined to a hemisphere to $2\theta = 60^{o}$ of single-crystal X-ray diffraction data collected on a variety of Oxford Diffraction instruments (Gemini, Xcalibur-1 and Super-Nova) with monchromatized MoKa radiation and CCD detectors. Refinements were performed on F^2 using SHELX (Sheldrick 2008) running under WinGX. The structures of the remaining three samples ($An_{78}Ab_{22}$, $An_{89}Ab_{11}$, $An_{96}Ab_{4}$) were taken from Angel et al. (1990). The Al/Si site occupancies of the tetrahedral sites T were obtained from the average <T-O> bond lengths determined by single-crystal structure refinements as $t_i = 0.25(1 + n_{An}) + (< T_i - O > - << T - O >>)/0.135$ (Kroll and Ribbe 1983; the coefficient of 0.135 comes from Angel et al., 1990). For $An_{60}Ab_{40}$ no *l* = odd reflections were

detected in the single-crystal X-ray diffraction patterns, and the structure was refined in space group $C\bar{1}$.

High-resolution powder X-ray diffraction patterns of each sample were collected on ESRF beamline ID31 (Fitch 2004) over the temperature range 298 to 935 K at steps of 3-5 K from 298 to 477 K and 10 K from 450 to 935 K. Each scan of a sample typically lasted less than 12 hours total. Powder diffraction measurements of high resolution, in terms of minimum instrumental contribution to the widths of the diffraction lines, were carried out at a wavelength of 0.40006(4) Å using an incident beam size of 2.0 mm^2 [2.0 mm (horizontally) × 1.0 mm (vertically)]. Each powdered sample (~ 10 mg) was loaded in a 1 mm Ø quartz capillary. Because data collection times for each whole pattern at a given temperature were less than 2 minutes, the samples were spun at high speed to ensure reasonable powder averaging. Measurements at temperatures between 298 and 477 K were performed using an Oxford Cryosystems 700-series nitrogen cryostream. Measurements at temperatures between 450 K and 935 K were performed using a hot air blower. Further details of the experimental setup are reported in Tribaudino et al. (2008).

Cell parameters were obtained by constrained sequential Rietveld analysis of the diffraction patterns, using the automatic sequential routine implemented in the EXPGUI-GSAS software package (Larson and Von Dreele 1997; Toby 2001). The background coefficients, zero shift, profile and unit cell parameters were refined independently for each pattern, using the results of the refinement at the previous temperature step as the initial model. Full refinement of all structural parameters was found to be unstable and to lead to unreliable unit-cell parameters in the automatic sequential mode, so atom positions were fixed in all refinements. The isotropic displacement parameters of all atoms were refined but with those of the tetrahedrally-coordinated cations constrained to be equal, as were those of the oxygen atoms. This provides a model for the intensities in the diffraction patterns that is physically reasonable (temperature induces greater changes in displacement parameters than in positional coordinates), allows for stable automated refinement, and does not bias the refined unit-cell parameters.

The Ab_{100} sample was also measured by single crystal X-ray diffraction to provide a cross-check on the temperature scale of the powder measurements. The experiment was done on a selected grain of albite (0.46 x 0.33 x 0.30 mm) showing sharp optical extinction with crossed polarized light under the microscope. Temperature calibration and description of the microfurnace as well as the experimental details of lattice parameter determinations are described in Cámara et al. (in prep). The unit-cell data of albite from single crystal diffraction were used to calibrate and check the temperature scale of the powder diffraction measurements. The single crystal volume data were fitted by a second order polynomial; the residuals in V/V_{303K} ranged between -0.0002 and +0.0003. The use of a higher-order polynomial did not improve the agreement. A comparison between the second-order polynomial from single crystal and powder diffraction data yielded differences in V/V_0 between -0.0009 and 0.0002. A negative difference greater than -0.0003 was found only in the range 380 - 500 K (powder data collected with the low temperature blower) and above 750 K. The deviation in volumes increases almost linearly with temperature and corresponds at most to ~-25 degrees at 500 K and -15 degrees at 950K. The data between 450 and 500 K from the heater, in the same range of the higher temperature data of the low temperature blower, agree within ± 0.0002 with the single crystal data. The temperatures of the powder data were therefore corrected by subtracting from the nominal temperature a value obtained by linear interpolation between 0 and 23 K from 380 to 500 K in the low temperature blower, and by 15K from 750 to 950 in the heater. After this correction the agreement against the albite single crystal data is better than ± 0.0002 in V/V_0, which is within the uncertainty of the single crystal data. It is believed that the correction for albite can be applied to all of the feldspar datasets as the identical experimental configuration was used for all and the same difference between low temperature heater and high temperature blower data between 450 and 500 K was found in all samples. The resulting lattice parameters from the powder diffraction and single crystal experiments are reported in Table 3 (deposited).

Results and Discussion

Structural state

The single-crystal structure refinements and the TEM observations of the samples, summarized in Table 1, and the room-temperature unit-cell parameters (Table 3) show that they are all "low plagioclase" with the highest degree of Al,Si order possible for each composition (Kroll 1983; Salje et al. 1985; Carpenter 1992). The increasing degree of disorder, as measured by decreasing values of Q_{od}, away from the end-members (Table 1) is solely due to the exchange of Al and Si with changing composition. For the purposes of thermal expansion measurements, all four samples Ab_{100}, $An_{27}Ab_{73}$, $An_{35}Ab_{65}$, $An_{46}Ab_{54}$ are considered to be "$C\bar{1}$ plagioclase" and the $An_{60}Ab_{40}$ and $An_{78}Ab_{22}$ samples to be $I\bar{1}$ plagioclase. The two most An-rich samples $An_{96}Ab_4$ and An_{100} have $P\bar{1}$ symmetry at room temperature, as result of a non-quenchable and fully reversible displacive phase transition between $P\bar{1}$ and $I\bar{1}$ symmetry at 514K and ~480 K respectively, which in the An_{100} sample gives rise to an excess volume contribution of about 0.1% (Figure 2) at room temperature. There is also evidence in the evolution of the unit-cell angles with temperature for a smeared version of this transition occurring in the $An_{89}Ab_{11}$ sample below 500K. The details of this transition will be analysed elsewhere (Tribaudino et al. in prep). As it is the $I\bar{1}$ phase that participates in metamorphic reactions, only the data collected above 550K from samples $An_{89}Ab_{11}$, $An_{96}Ab_4$ and An_{100} were used to determine their thermal expansion. Previous fits of volume variation of anorthite-rich feldspars ignore this transition (Skinner 1966, Czank and Shultz 1971, Berman 1988, Fei 1995, Gottschalk 1997, Holland and Powell 1998), leading to anomalously high volume thermal expansion coefficients and thus over-estimates of the volume of $I\bar{1}$ anorthites at higher temperatures.

With the exception of albite, there is very little change in the thermodynamic equilibrium state of Al,Si order at the temperatures achieved during the powder diffraction measurements (Salje et al., 1985; Carpenter, 1986; 1992). And, in the absence of water, the kinetics of Al/Si disordering below 950K are so slow (McConnell and McKie 1960; Carpenter et al. 1985; Carpenter 1986;

Wruck et al. 1991) that no change in Al/Si order will occur in the samples during the <12 hours of each powder diffraction measurement.

Volumes and excess volumes

Figure 2 shows the volume variation of the two end-member samples and, for clarity, just two of the intermediate compositions to indicate the general trends of behaviour. Two clear trends are immediately apparent. First, at room temperature, there is a significant difference of just under 1% between the molar or unit-cell volumes of albite and anorthite; most of this difference is the result of the anomalously small volume of albite compared to other $C\bar{1}$ feldspars (Figure 3). Second, the volume thermal expansion, represented by the slopes of the lines in Figure 2, decreases significantly with increasing anorthite content, confirming the qualitative picture presented by previous studies as summarised in Figure 1, and the recent data of Hovis et al. (2010). As a consequence, while at ambient temperature there is a significant excess volume of mixing (Figure 3), this decreases with increasing temperature so that by ~ 900 K all plagioclases have the same molar or unit-cell volume (Figures 2, 3). At higher temperatures the sense of volume difference between albite and anorthite is reversed with albite having the larger volume, and the excess volume of mixing becomes negative (Figure 3).

Volume thermal expansion coefficients

The volume thermal expansion coefficient α_V of a material is defined as $\alpha_V = 1/V\,(\partial V/\partial T)_P$, and is measured experimentally by the evolution of the sample volume (in practice the unit cell volume by diffraction) with temperature. If the volume thermal expansion coefficient α_V does not change with temperature, then integration gives:

1) $\ln(V/V_0) = \alpha(T-T_0)$,

First order truncation of this expression corresponds to the commonly reported $V/V_0 = \alpha(T-T_0)$ (e.g. Gottschalk 1997); the approximation is very close, so for practical use the values of α_V

derived by the two formulations are equal. Therefore we will refer to this model equation as "linear".

A non-linear behaviour of volume with temperature, and variation of α_V with temperature, is however always observed (e.g. Figure 2). This arises from changes in the vibrational behaviour of the atomic modes within the crystal. It can be modelled either with a physically consistent model involving the vibrational density of states (Suzuki et al. 1979, Anderson 1992), or by empirical models. Physical models, although they provide important information on the geophysical properties of minerals, require high quality data at low T, preferably close to 0K, and careful handling of the experimental parameters. Such data are seldom available for minerals and, for practical applications, an empirical model describing the evolution with temperature of the thermal expansion coefficient is sufficient.

Non-linear thermal expansion is in general fit by empirical polynomial equations (e.g. Berman 1988, Fei 1995, Holland and Powell 1998), such as the second order equation used by Berman (1988, hereinafter the "Berman" model):

2) $V/V_0= a_1(T-T_0)+a_2*(T-T_0)^2$

Taking the first derivative of this equation gives the thermal expansion coefficient as $\alpha_{V,T} = a_1 + 2a_2(T-T_0)$. Such a second-order polynomial predicts a linear increase in the thermal expansion coefficient, and does not reflect the practical observation that the thermal expansion rises to a limiting value at high temperature, because its temperature dependence is small above the Debye temperature (similar to the well-known behaviour of heat capacity; Pawley et al. 1996). The polynomial model can only achieve this behaviour with the addition of a further term, as in Fei (1995). Therefore, in the interests of simplicity, a single-parameter model adjusted to account for non-linear behaviour was proposed (Holland and Powell 1998, model as introduced in Pawley et al. 1996, hereinafter the "Holland-Powell" model), as follows:

3) $V/V_0= 1+a°(T-T_0)+20a° (\sqrt{T}-\sqrt{T_0})$

in which the thermal expansion at any given temperature can be obtained from $\alpha_T = a°(1-10/\sqrt{T})$.

The parameters for the three equations were obtained for all nine compositions by least-squares fitting to the V, T data and are reported along with room-temperature volume thermal expansion coefficients in Table 4. A reference temperature T_0 = 298 K was used and the volume at this temperature, V_0 was refined in all cases. As noted above, only data above 550K were used for the three most anorthite-rich samples, and the resulting parameters are therefore the volume, V_0, of the $I\bar{1}$ phase extrapolated to room temperature, and the thermal expansion coefficients of the $I\bar{1}$ phase.

In Figure 4, the fits of the volume data of $An_{27}Ab_{73}$ are shown as an example; the other datasets exhibit the same trends. Of the three models, the linear shows the poorest fit to the data. As it represents the average thermal expansion in the temperature range over which data were collected it overestimates the true volume thermal expansion at lower temperatures, and under-estimates it at higher temperatures (Figure 4), with the consequence that volumes calculated from the linear model will be increasingly under-estimated at increasing temperatures above 900K. The Holland-Powell model provides a significantly better fit, with more realistic volume thermal expansion coefficients at 300K (e.g. Figure 4) that are typically 30% smaller than those of the linear model (Table 4). However, it generally underestimates the volumes at higher temperatures, but not to such as great extent as the linear model (Figure 4). The Berman model provides the best statistical fit to the *V-T* data of all nine samples (Table 4), and appears to provide a reasonable model for volumes at metamorphic temperatures despite not modelling the saturation of thermal expansion (Figure 4). Irrespective of the values, the variation with composition of the fitted volume thermal expansion coefficients for all three models (Figure 5) shows the same patterns. The volume thermal expansion coefficient for albite is the highest, and the coefficient decreases with increasing anorthite content within the $C\bar{1}$ plagioclases up to $An_{50}Ab_{50}$. Within the $I\bar{1}$ plagioclases, with anorthite contents greater than $An_{50}Ab_{50}$, the variation in thermal expansion coefficient is much smaller. The small

increase seen for the Berman model at the most An-rich compositions may be an artefact introduced by only fitting the data above 550K, due to the presence at lower temperatures of the $P\bar{1} \leftrightarrow I\bar{1}$ phase transition. The fact that the volume compressibility of plagioclase is also largest for albite, and the compressibility also decreases more rapidly with anorthite content within the $C\bar{1}$ plagioclase than in the $I\bar{1}$ plagioclase (Angel 2004) suggests that the trends we have identified in thermal expansion with composition are real, and that both trends reflect the same underlying structural controls on the response of plagioclase feldspars to both temperature and pressure.

If the change in slope of the volume thermal expansion coefficient with composition on passing from $C\bar{1}$ to $I\bar{1}$ is ignored, then its value for a linear model can be represented by a second order polynomial fit:

$$\alpha_V = 2.90(4)\cdot10^{-5} - 3.0(2)\cdot10^{-7}*X_{An} + 1.8(2)\cdot10^{-9}*X_{An}^2$$

Here, and in the following, all nine values of α_V have been used in the fit, and X_{An} is given in mol%. For the Berman model the a_1 and a_2 parameters change with composition as:

$$a_1= 2.44(15)\cdot10^{-5} - 3.1(6)\cdot10^{-7}*X_{An} + 1.8(5)\cdot10^{-9}*X_{An}^2$$

$$a_2= 9(1)\cdot10^{-9} - 4(2)\cdot10^{-11}*X_{An}$$

And, for the Holland-Powell model the a° parameter (equation 3) varies with composition as:

$$a° = 4.96(5)\cdot10^{-5} - 4.7(2)\cdot10^{-7}*X_{An} + 2.2(2)\cdot10^{-9}*X_{An}^2$$

Anisotropy of thermal expansion

Because they have triclinic symmetry, the thermal expansion of plagioclase feldspars is allowed to be anisotropic. The anisotropy can most easily be represented by a "thermal expansion ellipsoid" (e.g. Nye 1957; Willaime et al. 1974; Ohashi and Finger 1973) which is simply the shape that a sphere made of the crystal attains after a change in temperature ΔT. The lengths of the principal axes of the ellipsoid are then $(1 + \alpha_i\Delta T)$ where the α_i are linear thermal expansion coefficients, so the directions of the major and minor axes of the ellipsoid are along the directions

of maximum and minimum thermal expansion in the crystal. The thermal expansion ellipsoid is thus a useful geometrical representation of the thermal expansion which is a second order tensor property. Because plagioclase feldspars are triclinic, there is no restriction on the magnitude, shape, or orientation of the ellipsoid. We therefore determined the ellipsoid for 369 data from our nine plagioclase samples by calculating the Lagrangian strain tensor between the unit-cell parameters measured at 550 K as a reference temperature, and at higher temperatures. The use of 550K as reference temperature makes it possible to compare the linear expansions and anisotropy for all samples on the same basis, without having to consider the significant influence of the $P\bar{1} \leftrightarrow I\bar{1}$ phase transition in the anorthite-rich samples (Figure 2).

The thermal expansion ellipsoid is very anisotropic in all plagioclase, with the direction of maximum thermal expansion (e_3) accounting for 70% or more of the total volume expansion (Fig. 6). This major deformation is more than twice that in the intermediate direction (e_2), whereas in the third direction (e_1), which is close to $[1\bar{3}2]$, the thermal expansion is quite small and negative. Anisotropy increases very slightly with anorthite content; in albite the ratio between the three principal axes of the strain is 1:0.43:-0.18, whereas in anorthite it is 1:0.32:-0.19. As the strain along e_1 is almost negligible, the thermal expansion can be described as essentially the expansion of the plane defined by the e_2 and e_3 axes. This anisotropy of thermal expansion is very similar in pattern to the anisotropy of expansion induced by exchange of the extra-framework cations. Because the direction of maximum expansion lies close to the (100) plane normal, the anisotropy has been attributed to the intrinsic flexibility of the "crankshaft chains" of tetrahedra that are the characteristic topology of the feldspar structure (e.g. Brown et al. 1984). Our results confirm the previous findings of Willaime et al. (1974) and Ohashi and Finger (1973). The same pattern of anisotropy occurs for the compression of alkali feldspars (e.g. Angel et al. 1989; Benusa et al. 2005; Nestola et al. 2008), but not for the compression of anorthite-rich plagioclase (e.g. Angel 1992), which points to the complexity of interactions between the tetrahedral framework and the extra-framework cations in determining the exact anisotropy of the structural changes of feldspars.

Although the orientation and anisotropy of the thermal expansion ellipsoid is similar for all plagioclase feldspars, further differences can be distinguished between the responses of the end members and those of the intermediate compositions. Intermediate plagioclases between $An_{27}Ab_{73}$ and $An_{89}Ab_{11}$ all have a very similar orientation of their strain ellipsoids, which rotate by a few degrees around e_3 during heating in a direction that parallels the rotation with increasing anorthite content (Figure 7). For these intermediate plagioclases the thermal expansion therefore mimics the strains induced by the compositional changes. By contrast, the orientation of the strain ellipsoid of albite is significantly different from that of other plagioclase, but with increasing temperature it rotates by about 15° degrees towards, but does not achieve by 935K, the orientation of intermediate plagioclase. Unlike the intermediate plagioclase, the anisotropy of expansion of albite increases with increasing temperature (Table 5). While the rotation of the thermal expansion ellipsoids of $An_{96}Ab_4$ and An_{100} continues the trend defined by the intermediate plagioclases, the direction of maximum expansion (e3) is rotated significantly farther away from [001], presumably as the result of the influence of the $P\bar{1} \leftrightarrow I\bar{1}$ phase transition that occurs at lower temperatures.

Conclusions

The general pattern of variation of volume thermal expansion coefficients α_V suggested in the older literature (as in Figure 1) and more recently by Hovis et al. (2010) is confirmed, with the values decreasing by a factor of approximately 2 from albite to anorthite, but our data place much tighter constraints on both the non-linearity of thermal expansion, and the numerical values of α_V. As a consequence, we have clearly demonstrated that the decrease in α_V with increasing anorthite content is greater within the albite-rich $C\bar{1}$ plagioclases than in the anorthite-rich $I\bar{1}$ plagioclases (Figure 5). These changes in volumetric response to temperature are the result of an isotropic change in the response of the feldspar structure (Figure 6); the strong (>70%) anisotropy of thermal expansion remains approximately constant across the entire plagioclase join, reinforcing the

previous interpretation that the anisotropy is an intrinsic property of the topology of the tetrahedral framework of all feldspars.

Acknowledgements

We are grateful to Michael Carpenter for supplying us with seven of the plagioclase samples used in this study. This work was supported in part by NSF in the form of grant EAR-0738692 to N.L. Ross and R.J. Angel. Fernando Cámara was supported by funding by CNR-IGG through the project TAP01.004.002. We thank the ESRF for beamtime on the high resolution powder diffraction beamline ID31.

References

Anderson OL, Isaak D, Oda HT (1992) High temperature elastic constant data on minerals relevant to geophysics. Rev Geophysics 30:57-92.

Angel RJ (1992) Order-disorder and the high-pressure $P\bar{1}$ - $I\bar{1}$ transition in anorthite. Am Mineral 77:923-929.

Angel RJ (2004) Equations of state of Plagioclase Feldspars. Contrib Mineral Petrol 146:506–512.

Angel RJ, Carpenter MA, Finger LW (1990) Structural variation associated with compositional variation and order-disorder behavior in anorthite-rich feldspars. Am Mineral 75:150–162

Beckenkamp J (1881) Uber die ausdehnung monosymmetrischer und asymmetrischer krystalle durch die würrme. Z Kristall 5:436-466.

Berman RG (1988) Internally-Consistent Thermodynamic Data for Minerals in the System Na_2O-K_2O-CaO-MgO-FeO-Fe_2O_3-Al_2O_3-SiO_2-TiO_2-H_2O-CO_2. J Petrol 29:445-522.

Brown WL, Openshaw RE, McMillan PF, Henderson CMB (1984) A review of the expansion behavior of alkali feldspars: coupled variations in cell parameters and possible phase transitions. Am Mineral 69:1058-1071

Carpenter MA (1986) Experimental delineation of the "e"= $I\bar{1}$ and "e" = $C\bar{1}$ transformations in intermediate plagioclase feldspars. Phys Chem Minerals 13:119-139

Carpenter MA (1992) Equilibrium thermodynamics of Al/Si ordering in anorthite. Phys Chem Minerals 19:1-24.

Carpenter MA, McConnell JDC, Navrotsky A (1985) Enthalpies of ordering in the plagioclase feldspar solid solution. Geochim Cosmochim Acta 49:947–966

Carpenter MA, Salje EKH, Graeme-Barber A (1998) Spontaneous strain as a determinant of thermodynamic properties for phase transitions in minerals. Eur J Mineral 10:621-691.

Carpenter MA, Salje EKH, Graeme-Barber A, Wruck B, Dove MT, Knight KS (1998) Calibration of excess thermodynamic properties and elastic constant variations associated with the alpha <-->beta phase transition in quartz. Am Mineral 83:2-22.

Czank M, Schultz H (1971) Thermal expansion of anorthite. Naturwissenschaften 58:94.

Fei Y (1995) Thermal Expansion. In "A handbook of physical constants, mineral physics and crystallography". Ahrens JA (ed). AGU Reference Shelf, 2, 29-44. ISBN 0-87590-852-7

Fitch AN (2004) The high resolution powder diffraction beam line at ESRF. J Res NIST 109:133-142.

Foit FF, Peacor DR (1973) The anorthite crystal structure at 410 and 830°C. Am Mineral 58:665-675.

Ghose S, McMullan RK, Weber HP (1993) Neutron diffraction studies of the P1–I1 transition in anorthite, $CaAl_2Si_2O_8$, and the crystal structure of the body-centered phase at 514 K. Z Kristall 204:215–237.

Gottschalk M (1997) Internally consistent thermodynamic data for rock-forming minerals in the system SiO_2 -TiO_2 -Al_2O_3 -CaO-MgO-FeO-K_2O-Na_2O-H_2O-CO_2. Eur J Mineral 9:175-223.

Grundy HD, Brown WL (1969) A high-temperature X-ray study of the equilibrium forms of albite. Mineral Mag 37:156-172

Grundy HD, Brown WL (1974) A high-temperature X-ray study of low and high plagioclase feldspars. In, W. S. MacKenzie and J. Zussman, Eds., Proc. N.A.T.O. Advanced Studies Institute on Feldspars, Manchester University Press, p. 162-173.

Holland TJB, Powell R (1998) An internally consistent thermodynamic data set for phases of petrological interest. J Metamorph Geol 16:309–343

Hovis GL, Graeme-Barber A (1997) Volumes of K-Na mixing for low albite-microcline crystalline solutions at elevated temperature: a test of regular solution thermodynamic models. Am Mineral 82:158-164.

Hovis GL, Medford A, Conlon M, Tether A, Romanoski A (2010) Principles of thermal expansion in the feldspar system. Am Mineral, submitted.

Knight KS, Price GD (2008) Powder neutron-diffraction studies of clinopyroxenes. I: the crystal structure and thermoelastic properties of jadeite between 1.5 and 270 K. Can Mineral 46: 1593 - 1622.

Kozu S, Ueda J (1933) Thermal expansion of plagioclase. Proc Imp Acad Tokyo 9:262-264.

Kroll H, Ribbe PH (1983) Lattice parameters, composition and Al, Si order in alkali feldspars. In Mineralogical Society of America: Rev Mineral, 2:57-99.

Kroll H, Bambauer HU and Schirmer U (1980) The high albite-monalbite and analbite-monalbite transitions. Am Mineral 65:1192-1211

Larson AC, Von Dreele RB (2004) General Structure Analysis System (GSAS). Los Alamos National Laboratory Report. LAUR 86-748 (2004).

McConnell JDC, McKie D (1960) The kinetics of the ordering process in triclinic $NaAlSi_3O_8$. Mineral Mag, 32,436-454.

Németh P, Tribaudino M, Bruno E, Buseck PR (2007) TEM investigation of Ca-rich plagioclase: Structural fluctuations related to the $I\bar{1}$-$P\bar{1}$ phase transition. Am Mineral 92:1080-1086.

Nestola F, Curetti N, Benna P, Ivaldi G, Angel RJ, Bruno E (2008) Compressibility and high-pressure behaviour of $Ab_{63}Or_{27}An_{10}$ anorthoclase. Can Mineral 46:1433-1454.

Ohashi Y (1982) A program to calculate the strain tensor from two sets of unit-cell parameters. In Hazen RM, Finger LW (eds) Comparative crystal chemistry. J. Wiley & Sons, Chichester, 92-102.

Ohashi Y, Finger LW (1973) Lattice deformations in feldspars. Carnegie Inst Wash YB 72:569-513.

Pawley AR, Redfern SAT, Holland TJB (1996) Volume behaviour of hydrous minerals at high pressure and temperature: 1. Thermal expansion of lawsonite, zoisite, clinozoisite and diaspore. Am Mineral 81:335–340.

Prewitt CT, Sueno S, Papike JJ (1976) The crystal structures of high albite and monalbite at high temperatures. Am. Mineral 6l:1213-1225.

Redfern SAT (1992) The effect of Al/Si disorder on the $I\bar{1}$ - $P\bar{1}$ co-elastic phase transition in Ca-rich plagioclase. Phys Chem Minerals 19: 246-254.

Redfern SAT, Salje EKH (1987) Thermodynamics of plagioclase. II. Temperature evolution of the spontaneous strain at the $I\bar{1}$ - $P\bar{1}$ phase transition in anorthite. Phys Chem Minerals 14: 189-195.

Redfern SAT, Graeme-Barber A, Salje EKH (1988) Thermodynamics of plagioclase III: Spontaneous strain at the $I\bar{1}$ - $P\bar{1}$ phase transition in Ca-rich plagioclase. Phys Chem Minerals 16:157-163.

Salje EKH (1985) Thermodynamics of sodium Feldspar. I: order parameter treatment and strain induced coupling effects. Phys Chem Minerals 12:93-98 .

Salje EKH, Kuscholke B, Wruck B, Kroll H (1985) Thermodynamics of sodium feldspar II: experimental results and numerical calculations. Phys Chem Minerals 12:99–107.

Saucier H, Saplevitch A (1962) La dilatation thermique des feldspaths. Norsk Geol Tidsskr 42:224-243.

Skinner BJ (1966) Thermal expansion. In: Handbook of Physical Constants (ed. Clark SP): Geological Society of America Memoir 97:75–96.

Stewart DB, Von Limbach D (1967) Thermal expansion of low and high albite. Am Mineral 52:389- 413.

Stewart DB, Walker GW, Wright TL, Fahey JJ (1966) Physical properties of calcic labradorite from Lake County, Oregon. Am Mineral 31:177-197.

Suzuki I, Okajima S, Seya K (1979) Thermal expansion of single-crystal manganosite. J Phys Earth 27:63-69.

Toby BH (2001) EXPGUI, a graphical user interface for GSAS. J Appl Crystall 34:210-213.

Tribaudino M, Benna P, Nestola F, Meneghini C, Bruno E (2005) Thermodynamic behaviour of the high temperature phase transition $P\bar{1} - I\bar{1}$ along the join An-SrF ($CaAl_2Si_2O_8$ – $SrAl_2Si_2O_8$). Phys Chem Minerals 32:314-321

Tribaudino M, Bruno M, Iezzi G, Della Ventura G, Margiolaki I (2008) The thermal behavior of richterite. Am Mineral 93:1659-1665.

Willaime C, Brown WL, Pernaud MC (1974) On the orientation of the thermal and compositional strain ellipsoids in feldspars. Am Mineral 59:45l-464.

Winter JK, Ghose S, Okamura FP (1977) A high-temperature study of the thermal expansion and the anisotropy of the sodium atom in low albite. Am Mineral 62:921-931.

Winter JK, Ghose S, Okamura FP (1979) A high-temperature structural study of high albite, monalbite, and the analbite - monalbite phase transition Am Mineral 64:409-423

Wruck B, Salje EKH, Graeme-Barber A (1991) Kinetic rate laws derived from order parameter theory IV: kinetics of Al,Si disordering in Na-feldspars. Phys Chem Minerals 17:700-710.

Table 1 Experimental data source for plagioclase and fitting models in thermodynamic data bases

	Database	Sample	Expansion coefficients (1/K)	Model	Formulation
albite	Holland and Powell (1998)	1	$4.56 \cdot 10^{-5}$	empirical	$V= V_0[1+a_0(T-T_0)-20a_0*(\sqrt{T}-\sqrt{T_0})]$
anorthite		2	$2.38 \cdot 10^{-5}$		
albite	Berman (1988)	1, 3	$26.307 \cdot 10^{-6}$ $32.407 \cdot 10^{-10}$	polynomial	$V= V_0[1+a_1(T-T_0)+a_2*(T-T_0)^2]$
anorthite		2, 5, 6	$10.918 \cdot 10^{-6}$ $41.985 \cdot 10^{-10}$		
albite	Gottschalk (1997)	7	$3.0 \cdot 10^{-5}$	linear	$V= V_0 + \alpha(T-T_0)$
anorthite		7	$1.6 \cdot 10^{-5}$		

References: 1: Winter et. al. (1979); 2: Grundy and Brown (1974); 3: Prewitt et al (1976); 4: Grundy and Brown (1974); 5: Foit and Peacor (1973); 6: Czank and Schultz (1971); 7: Skinner (1966), reports Kuzo and Ueda (1933); 8: Winter et al. (1977)

Table 2. Composition and structural state of the measured plagioclase samples.

An	Ab	Or	Sample ID	Source	Structural state	<<T-O>>	Qod	Single xtal
1	98	1	Amelia albite	VT museum	$C\bar{1}$	1.646	1.00 ($C\bar{1}$)	This work
27	71	2	97490b	P. Gay/USNM	$C\bar{1}$ + diffuse e	1.653	0.55 ($C\bar{1}$)	This work
35	64	1	91315b	Harker Collection	$C\bar{1}$ + diffuse e	1.656	0.35 ($C\bar{1}$)	This work
46	52	2	67783b	Harker Collection	$C\bar{1}$ + e + f	1.655	0.33 ($C\bar{1}$)	This work
60	39	1	67796b	Harker Collection	$I\bar{1}$ + e + f	1.664	0.26 ($C\bar{1}$)	This work
78	22	0	101377a	Harker Collection	$I\bar{1}$ +diffuse c	1.621 1.718	0.72 ($I\bar{1}$)	Angel et al. (1990)
89	11	0	87975b	Harker Collection	$I\bar{1}$ + streaked c	1.616 1.732	0.85 ($I\bar{1}$)	Angel et al.(1990)
96	4	0	115082a	Harker Collection	$P\bar{1}$	1.617 1.736	0.88 ($I\bar{1}$)	Angel et al. (1990)
100	0	0	Pale Rabbiose	M. Tribaudino	$P\bar{1}$	1.620 1.748	0.95 ($I\bar{1}$)	Angel et al. (1990)

Notes: Composition and structural state of $An_{46}Ab_{64}$ from Carpenter (1986), An_{100} Nemeth et al. (2007). All others were characterized and described in Carpenter et al. (1985). "Harker Collection" is the mineralogical collection of the Department of Earth Sciences, University of Cambridge, England. Pale Rabbiose (contact aureole of Monzoni intrusive complex, Trento, Italy) is probably the same geological provenance of Val Pesmeda/Val Pasmeda.

<<T-O>> is the grand-mean tetrahedral bond length for each sample. For An-rich plagioclases the average over the Al-rich and Si-rich sites is given separately

$Q_{od}(C\bar{1})$ defines the state of Al/Si order relative to completely-ordered albite. It is defined as $(t_{1o} - t_{1m})/(t_{1o} + t_{1m})$ as in Salje (1985), with site occupancies *t* obtained from the average <T-O> bond lengths determined by single-crystal structure refinements as $t_i = 0.25(1 + n_{An}) + (< T_i - O > - << T - O >>)/0.135$ (Kroll and Ribbe 1983; the coefficient of 0.135 comes from Angel et al. 1990). For $An_{60}Ab_{40}$ no *l* = odd reflections were detected in the single-crystal X-ray diffraction patterns, and the structure was refined in space group $C\bar{1}$.

Q_{od} ($I\bar{1}$) defines the state of Al/Si order relative to completely ordered anorthite as $(<< Al - O >> - << Si - O >>)/0.135$ (Angel et al. 1990).

Table 3:Electronic supplementary material: excel file showing measured unit cell parameters as a function of temperature for the nine plagioclase samples. All the cell parameters reported have an e.s.d. of 1 on the last digit.

Electronic supplementary material

Click here to download Electronic supplementary material: Table 3 cell parameters electronic supplementary material.xls

T (K) Ab0	a (A)	b (A)	c (A)	alpha (°)	beta (°)	gamma (°)	vol (A3)
298.7037	8.145	12.7938	7.1634	94.238	116.599	87.684	665.615
301.7761	8.1455	12.7947	7.1634	94.244	116.596	87.683	665.709
304.8781	8.1455	12.7942	7.1632	94.243	116.59	87.683	665.707
307.9509	8.1451	12.793	7.1628	94.244	116.588	87.678	665.577
311.0212	8.146	12.7945	7.1628	94.24	116.591	87.678	665.721
314.1094	8.1462	12.794	7.1636	94.238	116.589	87.679	665.798
317.1773	8.1466	12.7945	7.1634	94.242	116.585	87.678	665.87
320.2572	8.1461	12.7949	7.1629	94.24	116.584	87.681	665.809
323.333	8.1478	12.7952	7.1636	94.238	116.581	87.681	666.039
326.3915	8.1475	12.7944	7.1633	94.239	116.577	87.677	665.967
329.456	8.1476	12.7952	7.1634	94.233	116.574	87.68	666.043
332.5588	8.1485	12.7955	7.163	94.231	116.572	87.682	666.117
335.6157	8.1486	12.795	7.1631	94.232	116.571	87.677	666.105
338.6951	8.1485	12.7957	7.163	94.229	116.569	87.68	666.142
341.7866	8.1494	12.7953	7.163	94.233	116.567	87.677	666.208
344.8652	8.1497	12.7956	7.1633	94.228	116.566	87.679	666.277
347.9446	8.1501	12.7966	7.1634	94.221	116.564	87.68	666.388
351.0374	8.1506	12.797	7.1634	94.226	116.561	87.679	666.46
354.1018	8.1512	12.7964	7.1634	94.223	116.565	87.679	666.472
357.1606	8.1511	12.7962	7.1631	94.223	116.557	87.679	666.463
360.2729	8.1511	12.7972	7.1633	94.222	116.558	87.679	666.527
363.3239	8.1516	12.7969	7.1632	94.225	116.555	87.676	666.562
366.411	8.1523	12.7976	7.1633	94.215	116.553	87.679	666.677
369.4901	8.1524	12.7978	7.1632	94.22	116.546	87.674	666.729
372.5673	8.1525	12.7976	7.1632	94.218	116.548	87.676	666.718
375.6481	8.1526	12.7974	7.1634	94.216	116.546	87.678	666.751
378.7186	8.1534	12.7972	7.1629	94.21	116.544	87.675	666.778
378.6366	8.154	12.7985	7.1635	94.212	116.539	87.673	666.974
381.187	8.1536	12.798	7.1631	94.212	116.54	87.675	666.871
383.8071	8.1537	12.798	7.163	94.207	116.538	87.675	666.881
386.399	8.1545	12.7989	7.1635	94.212	116.537	87.676	667.044
388.9735	8.1547	12.7984	7.163	94.205	116.534	87.674	667.02
391.551	8.1557	12.7997	7.1636	94.205	116.534	87.674	667.222
394.1765	8.1551	12.7989	7.1634	94.205	116.53	87.675	667.137
396.7451	8.1552	12.799	7.1632	94.2	116.529	87.675	667.14
399.3231	8.1555	12.7989	7.1632	94.203	116.529	87.673	667.152
401.9149	8.1559	12.799	7.1633	94.202	116.525	87.674	667.223
404.4976	8.1568	12.7993	7.163	94.201	116.523	87.673	667.294
407.0847	8.1571	12.7998	7.1633	94.199	116.525	87.673	667.367
409.6687	8.1572	12.7997	7.163	94.198	116.519	87.671	667.369
412.2557	8.1569	12.7997	7.1631	94.194	116.521	87.673	667.358
414.8297	8.1576	12.8002	7.1634	94.2	116.518	87.669	667.482
417.395	8.1577	12.8006	7.1633	94.192	116.513	87.672	667.53
419.9678	8.1586	12.8002	7.1632	94.192	116.513	87.671	667.58
422.544	8.1592	12.8007	7.1635	94.191	116.513	87.67	667.685
425.1763	8.159	12.8006	7.1632	94.188	116.509	87.67	667.661

Table 4: calculated thermal expansion coefficients for plagioclase, V_{298} in Å^3. Volume thermal expansion coefficients α, a° and a_1 are to be multiplied by $10^{-5}K^{-1}$, and a_2 by $10^{-9}K^{-2}$. The coefficients for the samples $An_{89}Ab_{11}$, $An_{96}Ab_4$, and An_{100} were obtained from fits only to data above 550K, and thus apply to the $I\bar{1}$ phase.

	linear model			Holland-Powell model					Berman model				
	α_{298}	V_{298}	χ^2	α_{298}	α_{900}	a°	V_{298}	χ^2	$\alpha_{298} = a_1$	α_{900}	a_2	V_{298}	χ^2
Ab_{100}	2.89(1)	665.27(2)	0.020	2.10	3.33	4.995(8)	665.652(9)	0.009	2.45(2)	3.37	7.6(3)	665.52(1)	0.003
$An_{27}Ab_{73}$	2.21(1)	668.92(3)	0.037	1.61	2.54	3.82(1)	669.21(1)	0.008	1.64(2)	2.81	9.7(3)	669.25(1)	0.004
$An_{35}Ab_{65}$	2.04(1)	668.21(2)	0.024	1.48	2.35	3.53(1)	668.49(1)	0.007	1.62(2)	2.48	7.2(4)	668.46(2)	0.007
$An_{46}Ab_{34}$	1.93(1)	669.19(2)	0.029	1.41	2.22	3.34(1)	669.45(1)	0.014	1.43(2)	2.46	8.6(3)	669.49(1)	0.004
$An_{60}Ab_{40}$	1.71(1)	1339.14(4)	0.059	1.24	1.97	2.96(1)	1339.67(2)	0.024	1.34(1)	2.10	6.3(2)	1339.64(2)	0.009
$An_{78}Ab_{22}$	1.54(1)	1340.98(4)	0.076	1.12	1.76	2.65(1)	1341.39(2)	0.022	1.14(2)	1.94	6.6(3)	1341.44(3)	0.015
$An_{89}Ab_{11}$	1.64(1)	1339.91(9)	0.022	1.10	1.74	2.61(1)	1341.08(6)	0.012	0.88(6)	1.91	8.5(7)	1342.03(19)	0.005
$An_{96}Ab_4$	1.57(1)	1341.36(8)	0.015	1.05	1.67	2.51(1)	1342.49(5)	0.008	1.03(7)	1.77	6.2(8)	1342.88(21)	0.006
An_{100}	1.53(1)	1340.93(4)	0.004	1.03	1.62	2.44(1)	1342.03(3)	0.004	1.39(5)	1.59	1.7(6)	1341.32(15)	0.003

Table 5: Electronic supplementary material: excel file with the strain data. For each composition, from left to right: T (K), strain along ε_1, ε_2 and ε_3 axes, each followed by the error, the angles with crystallographic axes (in °) and the relevant errors, and x and y coordinate for stereographic projection, as in Ohashi (1982). The strain was calculated from 550 K to the given temperature, and reported in absolute values; in Fig. 6 the strain was instead given as per degree K.

Electronic supplementary material

Click here to download Electronic supplementary material: Table 5 axes of the thermal strain ellipsoid ELECTRONIC SUPPLEME

T Ab100	axis 1	err a1	and e1-a	erre1a	e1 - b	err e1-b	e1 ^ c	err e1 ^c
554	1.63E-08	1.90E-05	133.31	****	126.05	****	41.44	****
564	2.12E-05	1.23E-05	110.92	1.26	125.29	3.36	31.25	3.34
573	5.21E-05	1.25E-05	106.97	0.92	128.84	2.32	35.22	2.34
584	7.72E-05	1.17E-05	107.1	0.63	130.22	1.55	36.51	1.58
594	1.27E-04	1.17E-05	106.78	0.46	130.44	1.14	36.79	1.16
604	1.37E-04	1.29E-05	106.25	0.41	130.75	0.97	37.19	0.99
614	1.85E-04	1.18E-05	106.58	0.29	130.65	0.72	37.04	0.73
624	2.25E-04	1.13E-05	106.48	0.2	130.58	0.52	37	0.53
634	2.41E-04	1.19E-05	106.1	0.23	131.12	0.53	37.58	0.54
644	2.70E-04	1.30E-05	106.02	0.21	131.14	0.5	37.63	0.51
653	2.94E-04	1.09E-05	105.61	0.13	131.48	0.36	38.04	0.36
664	3.36E-04	1.08E-05	105.67	0.11	131.38	0.31	37.94	0.31
674	3.55E-04	1.19E-05	105.3	0.15	131.48	0.35	38.13	0.36
684	3.83E-04	1.75E-05	105.4	0.18	131.65	0.45	38.27	0.46
694	4.35E-04	1.09E-05	105.36	0.1	131.7	0.26	38.34	0.27
704	4.70E-04	1.70E-05	105.23	0.18	131.59	0.36	38.27	0.38
714	5.02E-04	1.16E-05	105.2	0.11	131.66	0.26	38.35	0.26
724	5.27E-04	1.08E-05	105.14	0.08	131.68	0.2	38.39	0.2
734	5.72E-04	1.18E-05	104.95	0.09	131.88	0.23	38.63	0.23
744	6.27E-04	1.21E-05	104.89	0.08	131.95	0.21	38.72	0.21
756	6.50E-04	1.76E-05	104.78	0.11	132.05	0.28	38.84	0.29
765	7.00E-04	1.27E-05	104.47	0.09	132.16	0.2	39.03	0.21
774	7.20E-04	1.05E-05	104.49	0.06	132.2	0.15	39.07	0.16
783	7.78E-04	1.18E-05	104.46	0.07	132.28	0.17	39.16	0.17
792	8.32E-04	1.72E-05	104.35	0.09	132.43	0.23	39.33	0.23
801	8.78E-04	1.16E-05	104.23	0.06	132.39	0.16	39.34	0.16
810	9.22E-04	1.17E-05	104.11	0.06	132.46	0.15	39.45	0.15
819	9.76E-04	1.45E-05	104	0.06	132.57	0.17	39.59	0.17
828	1.02E-03	1.06E-05	104.02	0.04	132.5	0.12	39.52	0.12
837	1.08E-03	1.27E-05	103.88	0.06	132.69	0.14	39.75	0.15
846	1.13E-03	1.70E-05	103.84	0.08	132.63	0.18	39.72	0.18
855	1.16E-03	1.19E-05	103.79	0.04	132.68	0.12	39.77	0.12
864	1.22E-03	1.65E-05	103.58	0.09	132.72	0.16	39.89	0.18
873	1.26E-03	1.05E-05	103.54	0.04	132.85	0.09	40.02	0.1
882	1.31E-03	1.68E-05	103.38	0.06	132.93	0.15	40.15	0.15
891	1.37E-03	1.08E-05	103.4	0.03	132.97	0.09	40.19	0.09
900	1.43E-03	1.66E-05	103.34	0.07	132.97	0.14	40.22	0.15
909	1.47E-03	1.27E-05	103.18	0.05	133.06	0.11	40.35	0.11
918	1.55E-03	1.25E-05	103.17	0.04	133	0.1	40.31	0.11
927	1.61E-03	1.15E-05	103.07	0.04	133.06	0.09	40.41	0.1
936	1.67E-03	1.41E-05	103.05	0.05	133.09	0.11	40.45	0.11
T An27Ab	axis 1	err a1	and e1-a	erre1a	e1 - b	err e1-b	e1 ^ c	err e1 ^c
554	1.26E-07	1.12E-05	83.36	****	12.56	****	86.19	****
564	6.51E-06	1.57E-05	99.62	4.63	133.35	6.57	41.65	7.43
574	3.50E-05	9.45E-06	97.79	1.18	135.09	2.02	43.88	2.22
584	6.03E-05	1.30E-05	98.09	1.15	135.12	1.92	43.79	2.12
594	8.35E-05	1.49E-05	96.35	1.19	136.45	1.69	45.67	1.96
604	1.05E-04	1.10E-05	97.05	0.47	135.81	0.96	44.82	1.02
614	1.33E-04	9.18E-06	96.82	0.41	135.87	0.67	44.98	0.74
624	1.64E-04	1.02E-05	97.38	0.4	135.83	0.63	44.72	0.7

Figure captions

Figure 1: Previous measurements of the volume thermal expansion of plagioclase. The data from the original papers were refit with a linear model. Open circle: Von Limbach and Stewart (1967); large open square Kozu and Ueda (1933); open diamonds: Grundy and Brown (1974); open diamond, bold: Grundy and Brown (1969); open circle: Winter et al. (1977); full diamond: Stewart et al. (1966); cross: Carpenter (1992); open square: Czank and Shultz (1971). For albite, only data for low albite are plotted; high albite thermal expansion is very similar to that of low albite (Prewitt et al. 1976, Winter et al. 1979).

Figure 2. Evolution of unit-cell volumes of four of the samples with temperature. One-half of the true unit cell volumes of $An_{60}An_{40}$ and An_{100} $I\bar{1}$ plagioclases have been plotted. Note the additional volume decrease in An_{100} at low temperatures as a result of the $I\bar{1}$ to $P\bar{1}$ displacive phase transition. Lines are the Holland-Powell model for thermal expansion fit to the data.

Figure 3: Experimental unit-cell volumes of all samples at three selected temperatures (diamonds). One-half of the true unit cell volumes of the $I\bar{1}$ plagioclases have been plotted. A second order polynomial fit of the volumes calculated using linear (red), Berman (black) and Holland-Powell (blue) models is shown for comparison; changes in cell volume with temperature and composition according to Holland-Powell model are also extrapolated to 1200 and 1500K

Figure 4: Changes in cell volume (left) and α_V (right) with temperature in $An_{27}Ab_{73}$. Lines are fits of different models to the data: red, linear (L); blue, Holland-Powell (H-P); black: Berman (B). The thermal expansion data in the right-hand figure, with error bars, were calculated by fitting the linear volume variation with temperature over 100 K increments.

Figure 5. Variation of the volume thermal expansion coefficient at 300K with composition in plagioclase for the linear model (red, open diamond, on top), the Holland-Powell model (blue, full diamond) and the Berman model (black, open diamond). The values of all coefficients are given in Table 4.

Figure 6. Axial thermal expansion coefficients in plagioclase.

Figure 7. Stereographic projection of the axes of the strain ellipsoid calculated at 550 K as reference starting state; axes are projected in the upper hemisphere. The orientation of the crystallographic axes is that of $An_{89}Ab_{11}$. Data for $T > 550$ K are reported. The arrows indicate the direction of increasing anorthite content, which for a given sample are also those of increasing temperature.

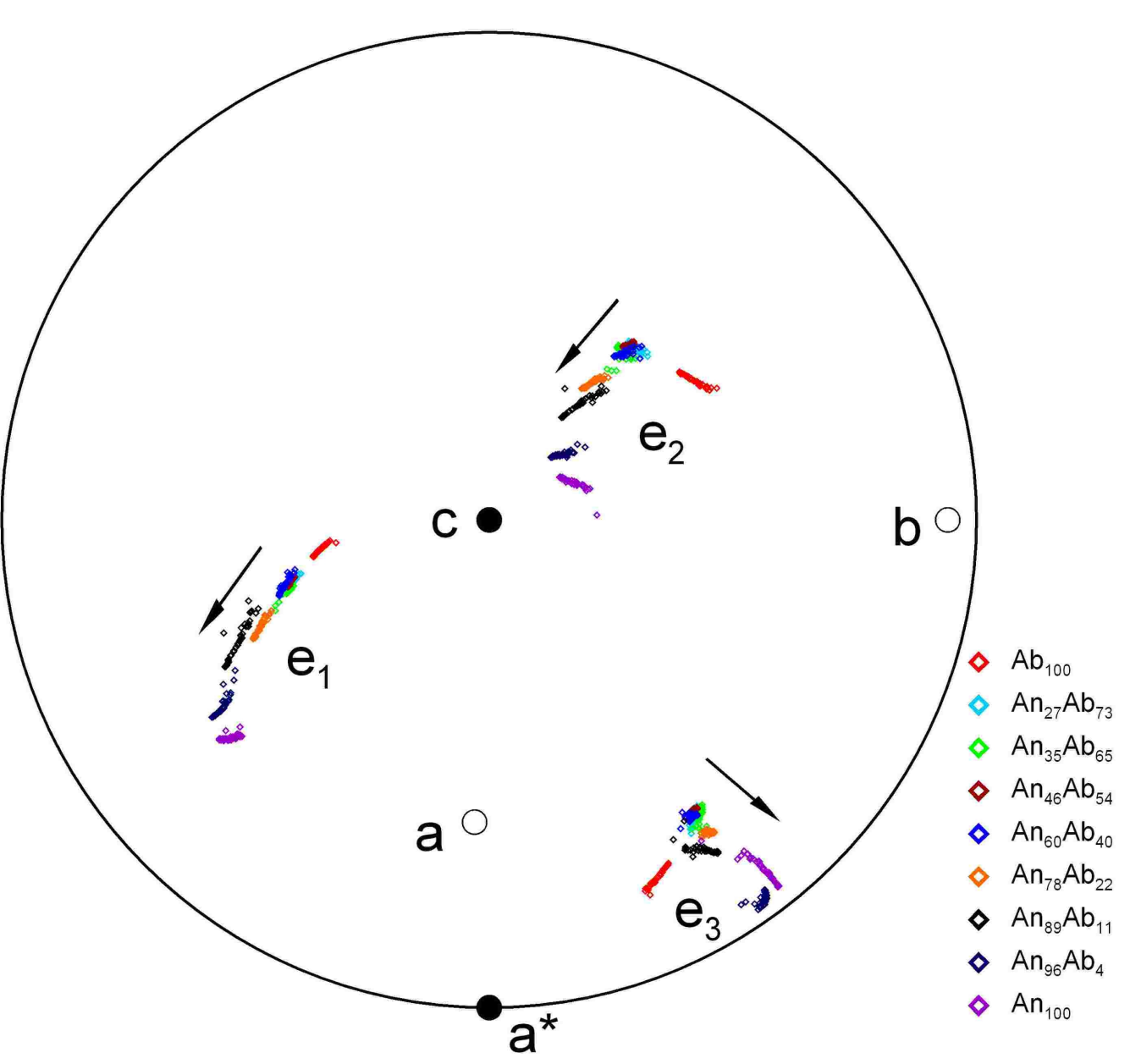
e2
c
b
e1
a
e3
a*
Ab100
An27Ab73
An35Ab65
An46Ab54
An60Ab40
An78Ab22
An89Ab11
An96Ab4
An100

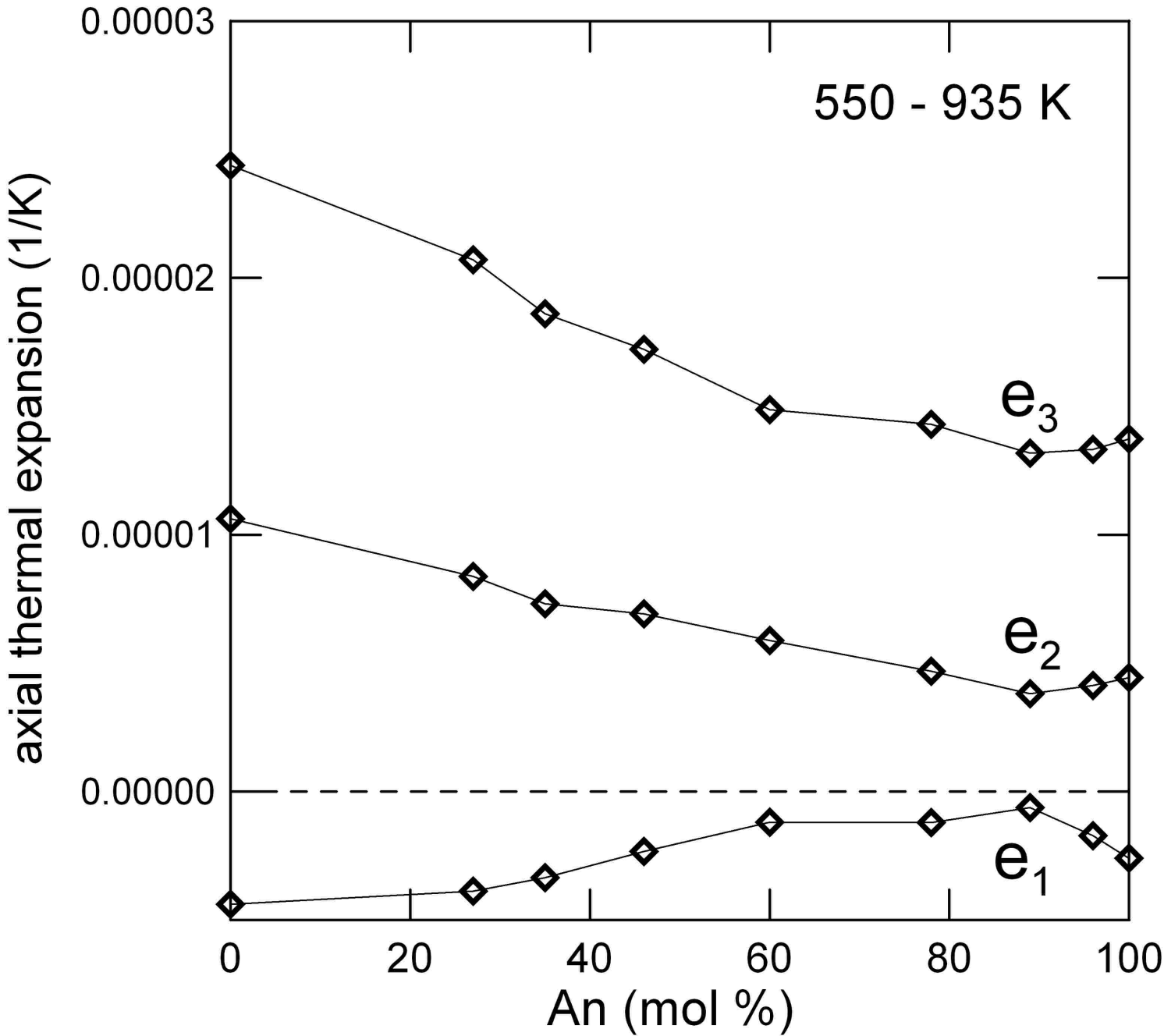
0.00003
0.00002
0.00001
0.00000
axial thermal expansion (1/K)
550 - 935 K
e3
e2
e1
0
20
40
60
80
100
An (mol %)

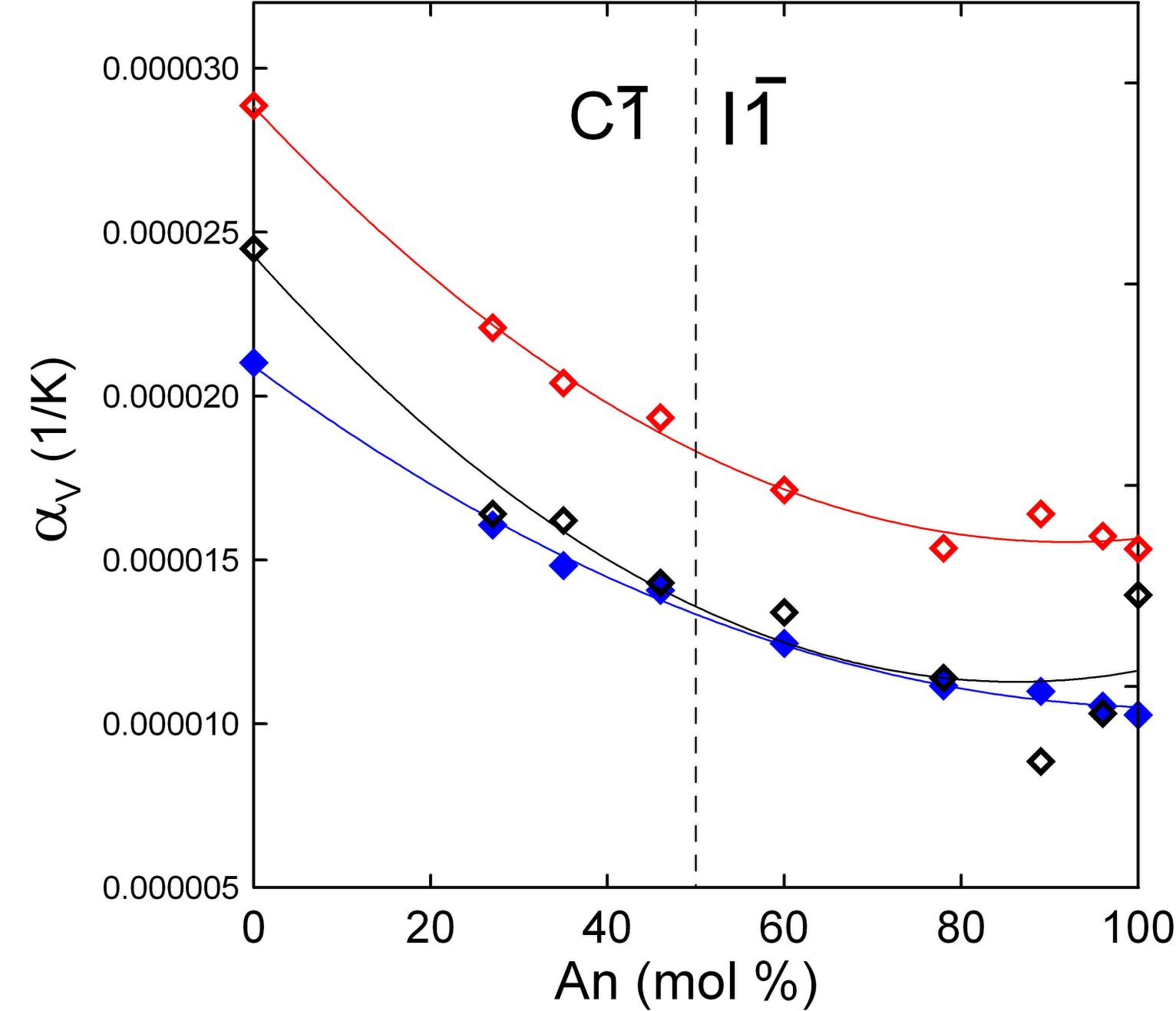
0.000030
0.000025
0.000020
0.000015
0.000010
0.000005
α_V (1/K)
0
20
40
60
80
100
An (mol %)
C$\bar{1}$
I$\bar{1}$

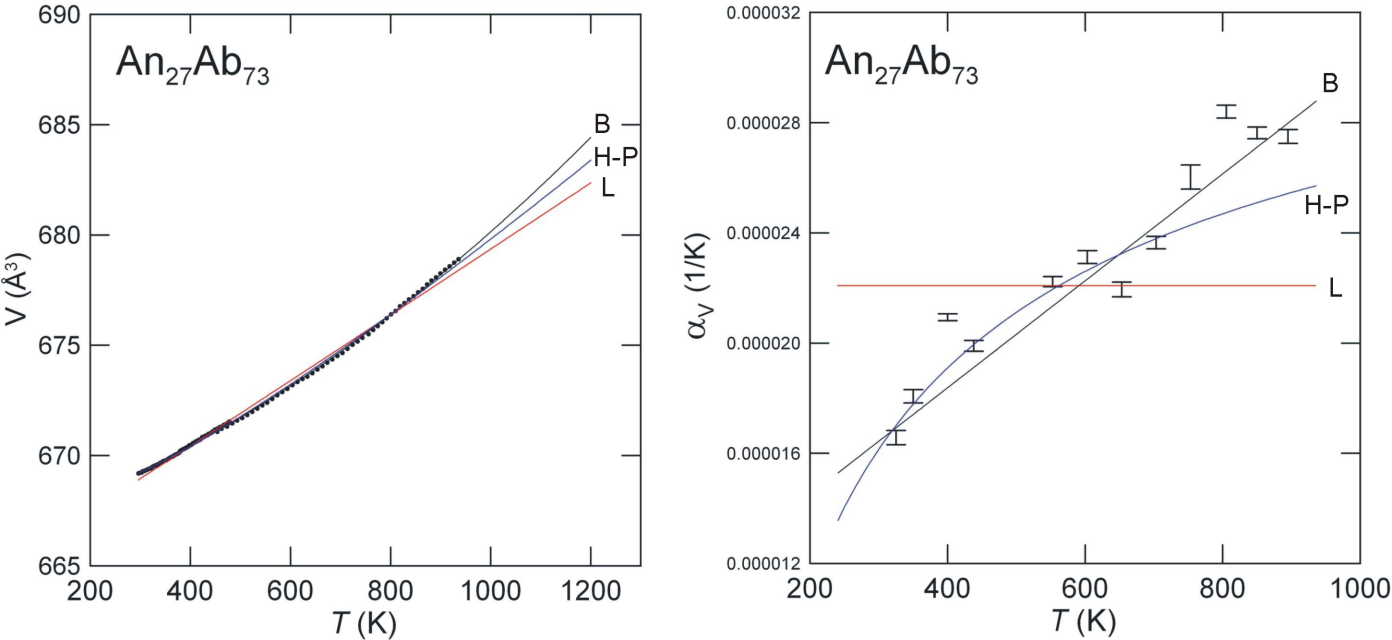
An27Ab73
B
H-P
L
V (Å3)
T (K)
690
685
680
675
670
665
200
400
600
800
1000
1200
An27Ab73
B
H-P
L
αV (1/K)
T (K)
0.000032
0.000028
0.000024
0.000020
0.000016
0.000012
200
400
600
800
1000

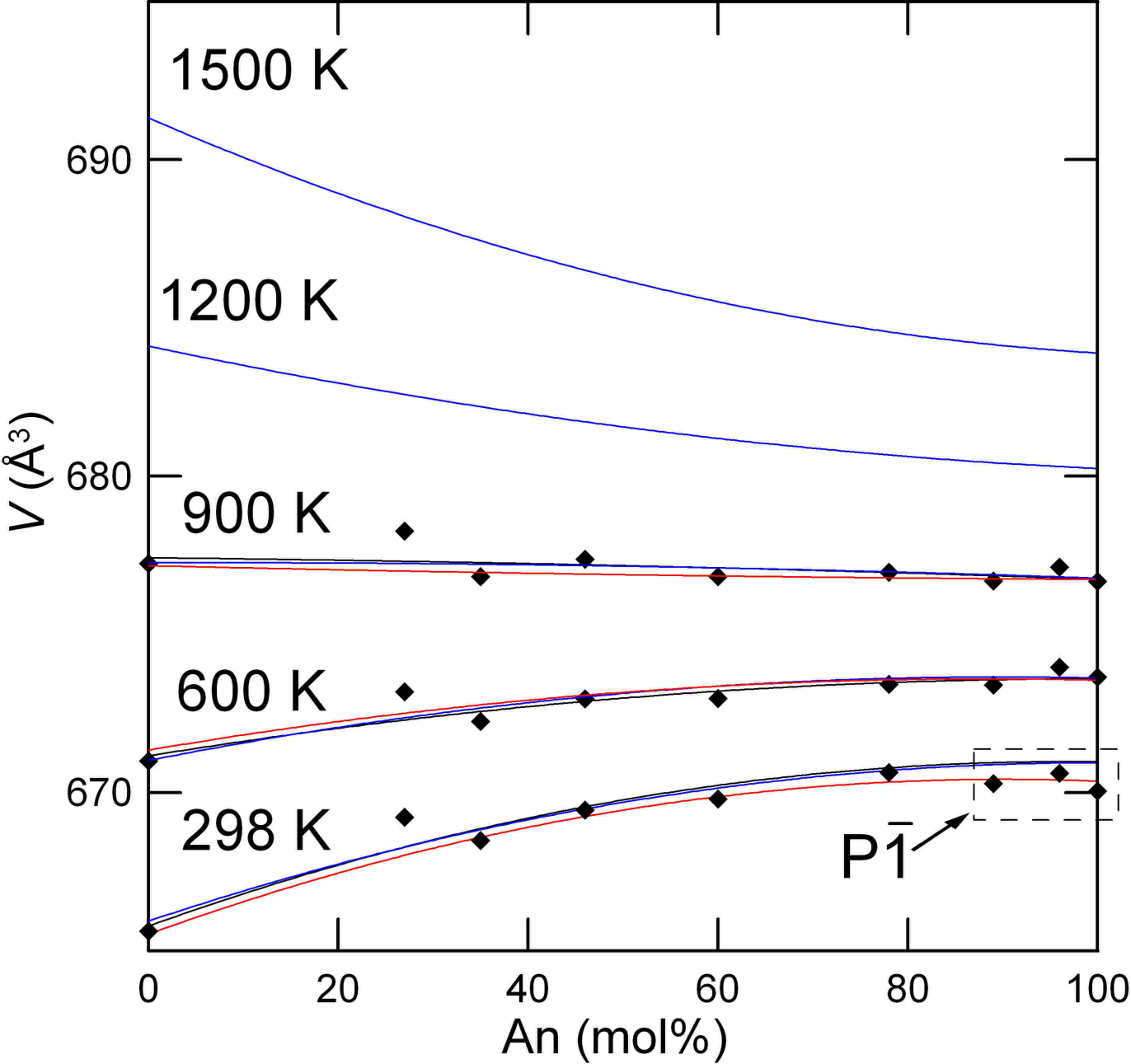
1500 K
1200 K
900 K
600 K
298 K
P1̄
690
680
670
V (Å3)
0
20
40
60
80
100
An (mol%)

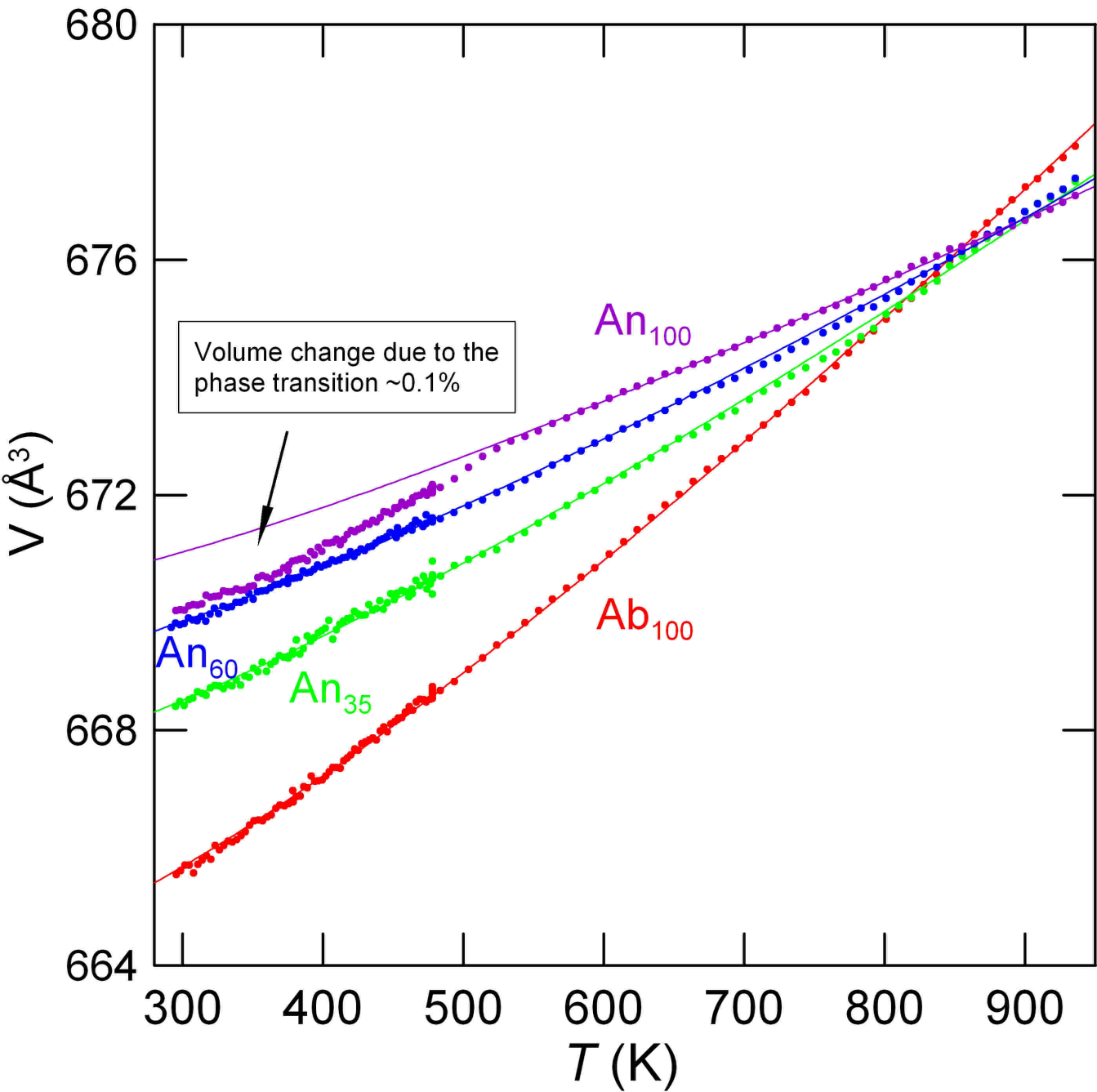
680
676
672
668
664
V (Å3)
300
400
500
600
700
800
900
T (K)
Volume change due to the
phase transition ~0.1%
An100
An60
An35
Ab100

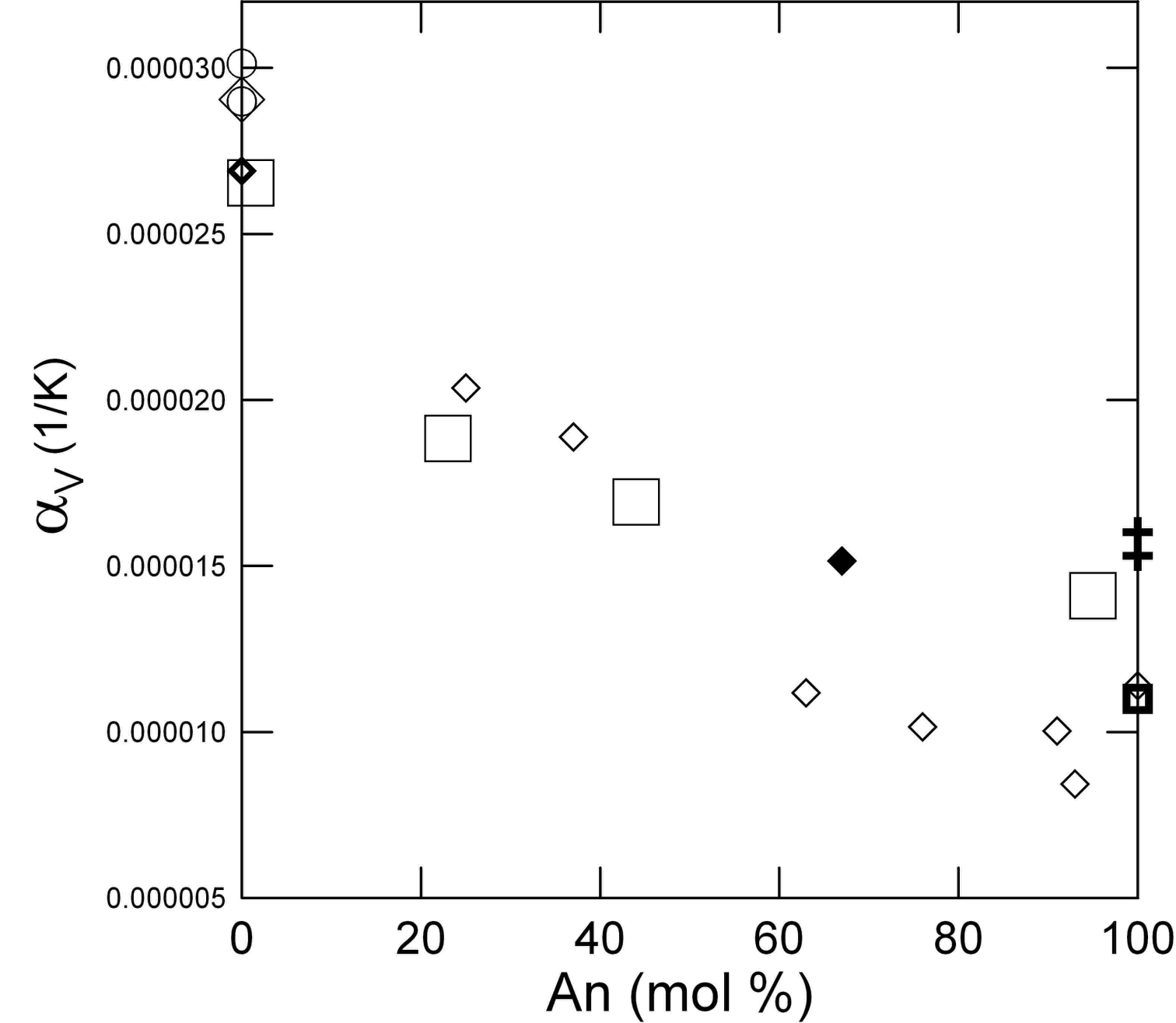
0.000030
0.000025
0.000020
0.000015
0.000010
0.000005
α_V (1/K)
0
20
40
60
80
100
An (mol %)